Mingyang Yang

Xinqian Zheng
e-mail: zhengxq@tsinghua.edu.cn

Yangjun Zhang

State Key Laboratory of
Automotive Safety and Energy
Tsinghua University,
Beijing 100084, China

Takahiro Bamba

Hideaki Tamaki

Turbo Machinery and
Engine Technology Department,
IHI Corporation,
Yokohama, 235-8501, Japan

Joern Huenteler
RWTH Aachen University,
Aachen 52056, Germany

Zhigang Li
Beijing Special Vehicle Institute,
Beijing 100072, China

Stability Improvement of High-Pressure-Ratio Turbocharger Centrifugal Compressor by Asymmetric Flow Control—Part I: Non-Axisymmetrical Flow in Centrifugal Compressor

This is Part I of a two-part paper documenting the development of a novel asymmetric flow control method to improve the stability of a high-pressure-ratio turbocharger centrifugal compressor. Part I focuses on the nonaxisymmetrical flow in a centrifugal compressor induced by the nonaxisymmetrical geometry of the volute while Part II describes the development of an asymmetric flow control method to avoid the stall on the basis of the characteristic of nonaxisymmetrical flow. To understand the asymmetries, experimental measurements and corresponding numerical simulation were carried out. The static pressure was measured by probes at different circumferential and stream-wise positions to gain insights about the asymmetries. The experimental results show that there is an evident nonaxisymmetrical flow pattern throughout the compressor due to the asymmetric geometry of the overhung volute. The static pressure field in the diffuser is distorted at approximately 90 deg in the rotational direction of the volute tongue throughout the diffuser. The magnitude of this distortion slightly varies with the rotational speed. The magnitude of the static pressure distortion in the impeller is a function of the rotational speed. There is a significant phase shift between the static pressure distributions at the leading edge of the splitter blades and the impeller outlet. The numerical steady state simulation neglects the aforementioned unsteady effects found in the experiments and cannot predict the phase shift, however, a detailed asymmetric flow field structure is obviously obtained. [DOI: 10.1115/1.4006636]

1 Introduction

The history of turbocharging is almost as old as that of the internal combustion engine. A turbocharger consists of a compressor and a turbine. The compressor is driven by the turbine extracting energy from exhaust gases. Compared to a naturally aspirated engine, the benefits of a turbocharged engine are increased power, lower fuel consumption, and reduced emissions [1,2].

High-pressure-ratio turbocharging technology is the developing trend of turbocharged internal combustion engines due to the following reasons: 1) significant downsizing to mitigate CO_2 emission and reduce fuel consumption [3], 2) satisfying rigid future emission regulations, i.e., NO_x treatment by engine control means high rates of exhaust gas recirculation (EGR) [3,4], and 3) the facilitation of high altitude operation [5]. However, a high pressure ratio causes the flow in the compressor to be transonic. Hence, the stable flow range is narrowed, since the stall incidence decreases with an increased relative Mach number at the inlet of the impeller [6]. Therefore, map width enhancement is a major issue for state-of-the-art high-pressure-ratio compressor design and development.

A turbocharger centrifugal compressor comprises an impeller, a diffuser, and a volute. While the former two are periodically symmetric in the circumferential direction, the volute is asymmetric due to its gas-collection function. It is usually designed as a spiral-collection overhung housing that collects the air from the diffuser and passes it to the pipe system. It has been recognized that the improvement of centrifugal compressor performance requires a good understanding of the flow mechanisms inside the volute [7–9]; especially the interaction among the volute-diffuser-impeller [10,11]. The volute is mostly designed in a way to shape a uniform circumferential static pressure distribution both in the volute and the diffuser. However, the volute acts as a diffuser at lower than the design flow rate and acts as a nozzle at higher than the design flow rate, respectively. A number of authors have researched this subject. It has already been confirmed that the asymmetrical configuration has a significant impact on the flow field in the diffuser and in the impeller [12,13]. This circumferential asymmetry has been recognized and intensive experimental investigations of the flow within the volute and the propagation of the distortion into upstream components were carried out for subsonic compressor units [14,15].

The work of Sorokes et al. confirmed that the pressure nonuniformity extended upstream of the impeller, implying that the impeller was subjected to varying inlet and exit conditions. The computational fluid dynamics (CFD) results further implied that the inlet flow distortion caused a large leading edge pressure differential along with a large negative incidence, which may induce a flow separation and thus a very disturbed flow field in the impeller [14]. A three-dimensional unsteady analysis of the flow in the impeller with circumferential distortion of the outlet static pressure was investigated using a numerical method by Fatsis et al. [16]. The perturbation was thus propagated upstream from the impeller outlet and influenced the incidence at the blade leading edges and other flow parameters. Gu et al. [10,11] found that the

Contributed by the International Gas Turbine Institute (IGTI) of ASME for publication in the JOURNAL OF TURBOMACHINERY. Manuscript received April 26, 2010; final manuscript received December 26, 2011; published online November 1, 2012. Assoc. Editor: Michael Casey.

performance parameters of the single impeller passage differed because of the asymmetric flow at the outlet of the impeller. There was almost no phase shift between the distortion in the diffuser and impeller according to their results, and it was considered that the unsteady effects of the volute-impeller interaction can be neglected when the Strouhal number is small enough.

Little detailed measurement was carried out in the impeller to investigate the asymmetric flow. Furthermore, to the authors' knowledge, very little research work has been focused on the impact of the volute on the flow field in a high-pressure-ratio turbocharger centrifugal compressor. The purpose of this two-part paper is first to understand the asymmetry of flow field due to the asymmetric geometry of the volute and, subsequently, to develop a novel asymmetric flow control method to widen the stable flow range of a turbocharger centrifugal compressor with a high-pressure-ratio, the narrowing flow range of which is of utmost importance for its application. In Part I, the nonaxisymmetrical flow characteristics in the high-pressure-ratio turbocharger centrifugal compressor are investigated by using experimental and numerical means, the results of which are the basis for the work presented in Part II.

2 Experiment Facilities

The measurements were performed on a turbocharger testing facility. Key geometries and operational characteristics of the investigated centrifugal compressor are listed in Table 1. The configuration of the volute was overhung with an elliptic cross-section.

In order to investigate the static pressure distribution in the compressor, 41 measurement points were positioned in both the meridional and streamwise directions. Figures 1(*a*)–1(*c*) shows the locations of the probes in the compressor. In the streamwise direction, probes were located in the shroud in the vicinity of the leading edge of the main blades and splitter blades, respectively, as shown in Fig. 1(*a*). Two other streamwise positions were located at the inlet and outlet of the vaneless diffuser, as shown in Fig. 1(*b*). For each streamwise position in the impeller and diffuser, eight static pressure probes were mounted in an equidistant circumferential distribution. Nine pressure probes were mounted in the wall of the volute, as shown in Fig. 1(*c*). The circumferential angle of the position of the volute tongue is around 47 deg. The distribution of static pressure in the circumferential direction throughout the compressor was obtained by the arranged probes with an error of less than ±0.2%.

3 Numerical Methods

In order to investigate the detailed flow field in the compressor, a numerical simulation was employed. The CFD solver EURANUS (NUMECA) is employed to solve the Reynolds-averaged Navier-Stokes equations in a conservative formulation based on a 3-D steady compressible finite volume scheme. A central scheme was used for the spatial discretization and the four-stage Runge-Kutta scheme was used for the temporal discretization. The Spalart-Allmaras (S-A) 1-equation model was applied for turbulence closure [17]. The model features numerical accuracy for the calculation of the viscous boundary layer turbulent flow, separated flows of small or medium scale, and free shear turbulent flow, except for jet flows [18]. The global residual as 10^{-5} is taken as the convergence criterion for operating points away from surge. The numerical failure point at the small mass flow rate is taken as the surge point.

Table 1 Centrifugal compressor geometry

Design rotational speed, N	65,000 rpm
Design mass flow rate	1.3 kg/s
Exit blade angle (meridional)	−38 deg
Impeller inlet tip diameter, D_1	110 mm
Impeller outlet diameter, D_2	150 mm
Blade number	9/9 main/splitter blades
Diffuser exit diameter, D_5	228 mm
A/R (volute)	26.23 mm

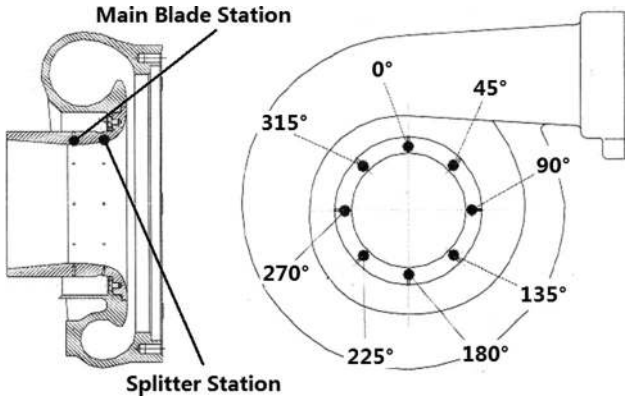

Fig. 1 Measurement positions in the investigated compressor: (*a*) measurement in the impeller, (*b*) measurement in the diffuser, and (*c*) measurement in the volute

All passages of the impeller, the vaneless diffuser, and the volute were modeled in the simulation. The computational domain in the region upstream of the impeller was extended, as shown in Fig. 2(*a*). The cell number for a single passage is around 650,000, which is large enough to guarantee the predicted result to be independent from the cell number, according the grid number independence investigation. There are 17 cells in the spanwise direction for the blade tip clearance model. Butterfly mesh is used for the tip model to obtain good mesh quality. The size of the first cell near wall in the impeller and the volute is set as 0.001 mm and 0.01 mm, respectively, which guarantees the y^+ is small enough for the S-A turbulence model. The whole domain consisted of approximately 6,500,000 nodes. The grid exhibits acceptable qualities, as defined by measures of the orthogonality, expansion ratio, and the aspect ratio. To mesh the overhung volute, a butterfly mesh was applied in order to augment the orthogonality of boundary layer cells. In Fig. 2(*a*), the mesh of the passage projected on the rotating solid walls is shown with the important entities marked. In Fig. 2(*b*), a cross-section of the volute exit mesh is displayed in order to point out the butterfly mesh approach. Figure 2(*c*) shows the volute mesh and passage numbering.

The total temperature and total pressure, together with the velocity direction, were imposed as the inlet boundary conditions; static pressure was set as the outlet boundary condition. No-slip and impermeability conditions were imposed on the solid walls. The interface between the impeller and volute was modeled as a frozen rotor, since angular variations of the flow quantities exceed a negligible level and are the objective of this research work. Thus, the rotating system was calculated in relative coordinates, yet the flow quantities are locally transferred without varying the relative position of the impeller and the volute. To quantify the effect of the relative position on the simulation results, three different positions of the impeller were modeled and analyzed. The periodicity of the impeller passage is 40 deg; thus, the rotor was moved from angle φ to $\varphi + 13.3$ deg and $\varphi + 26.67$ deg, respectively. The performance results of the three different conditions at design speed are shown in Fig. 3(*a*). The total to total pressure ratio and total to total efficiency are hardly influenced by the positions. Figures 3(*b*) and 3(*c*) show the static pressure distribution in the circumferential direction at the diffuser outlet and the impeller outlet for three positions. Little difference is noticed among the distributions at the three positions. It is implied that the distortion of the distribution comes from the volute instead of the impeller, which will be analyzed in the following text. It is further

implied that neglecting the influence of the relative position of the impeller and the volute is reasonable for the flow detail investigation. The position shown in Fig. 2(*c*) is chosen for the investigation in the paper.

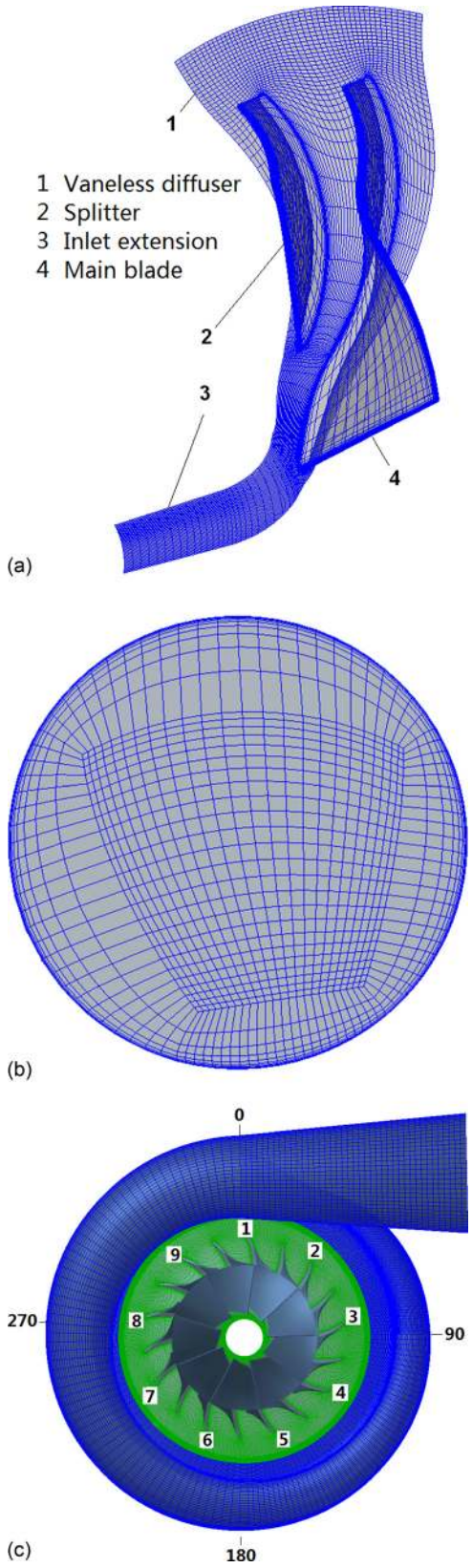

Fig. 2 Created mesh in detail: (*a*) passage mesh projected on solid walls, (*b*) butterfly meshing approach in volute cross-section, and (*c*) volute mesh and passage numbering

4 Results and Analysis

4.1 Experimental Results

4.1.1 Testing Points and Compressor Performance. The static pressure distribution at different flow rates and speeds was measured on the testing facilities. Four speed lines, i.e., 45,000 rpm (69.2% *N*), 55,000 rpm (84.6% *N*), 65,000 rpm (100% *N*), and 68,000 rpm (105% *N*) will be discussed. The speeds and mass flow rate are dimensionless by the design rotational speed *N* and the design flow rate, respectively. Three operating points on each line were chosen for analysis, which represent the highest efficiency condition, the highest flow rate condition (near choke), and the lowest mass condition (near surge). The points are shown in Fig. 4.

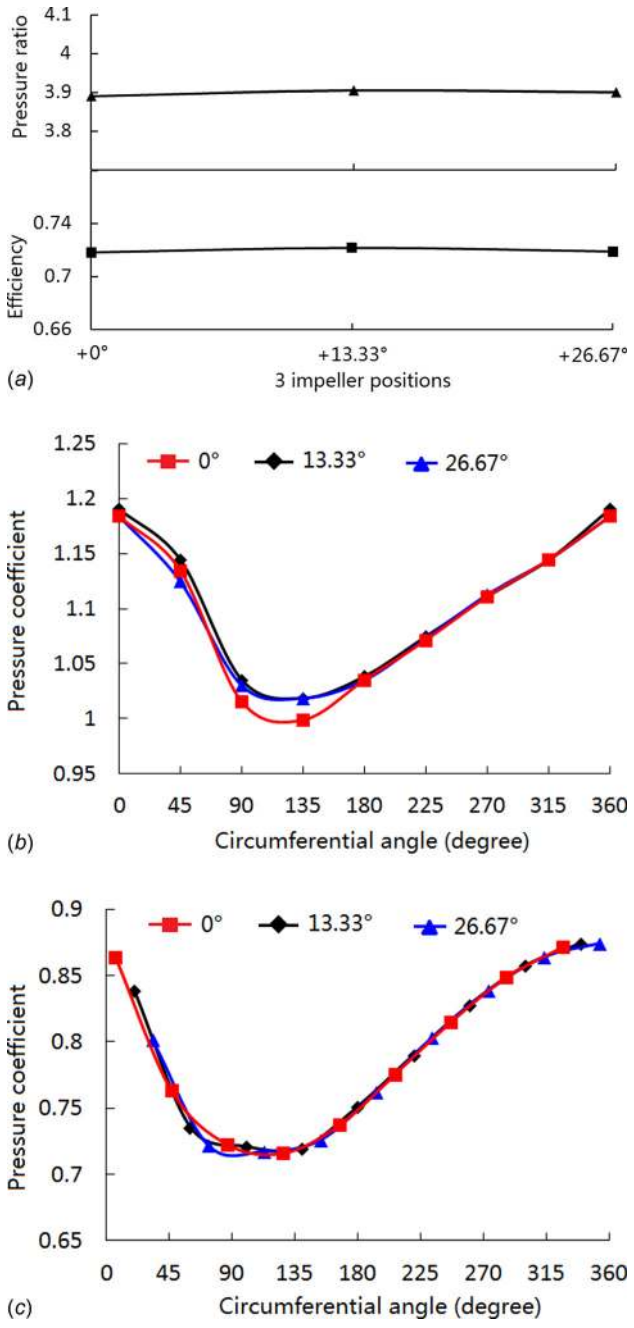

Fig. 3 Influence of the relative position of the impeller and volute on performance:(*a*) compressor performance,(*b*) pressure coefficient at the diffuser outlet, and(*c*) pressure coefficient at the impeller outlet

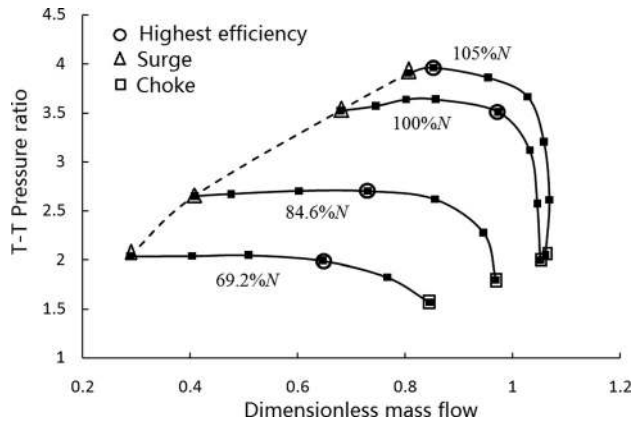

Fig. 4 Measured compressor performance

4.1.2 The Pressure Distribution in the Volute. The pressure coefficient distribution in the volute at design rotational speed is shown in Fig. 5. The coefficient PC is defined as follows

$$PC = \frac{P}{\rho_{in} U_2^2} \tag{1}$$

The parameter is a dimensionless static pressure in which the effect of rotation is included. The detailed measuring points can be seen in Fig. 1(*c*). It can be seen from the figure that the circumferential static pressure coefficient variations are quite different for the three operating conditions. Usually, a volute is designed as a tube in which the velocity of the air remains nearly constant at the design point or the point of highest efficiency. Therefore, the static pressure distribution at the highest efficiency point is relatively flatter than other operating conditions, as shown in Fig. 5. However, as the compressor approaches the surge condition, the flow is decelerated in the volute and it acts as a diffuser because of the reduced flow rate. As a result, the static pressure in the volute increases from the tongue to the compressor outlet. On the contrary, when the compressor approaches the choke point, the static pressure in the volute decreases due to the function of the volute as a nozzle. Hillewaert et al. [12] and Hagelstein et al. [19] reported similar results in the volute (diffuser exit).

4.1.3 The Pressure Distribution in the Diffuser. The pressure coefficient distribution in the diffuser is shown in Figs. 6 and 7 at two rotational speeds (69.2% N and 100% N). At both operating conditions, near surge and near choke, similar trends are present in the diffuser for both rotational speeds. Near surge, there is a remarkable region of pressure coefficient distortion with a minimum

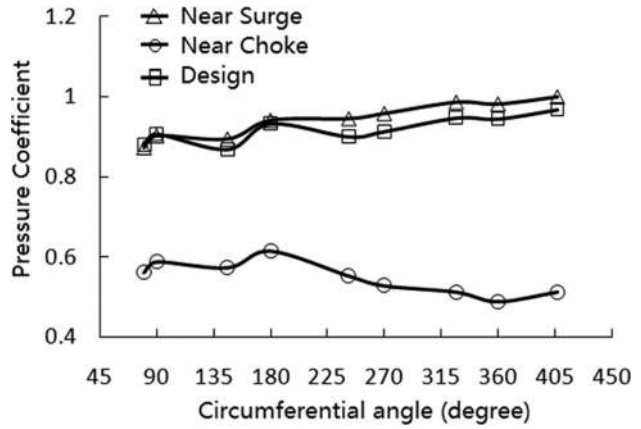

Fig. 5 Static pressure distribution in the volute at 100% *N*

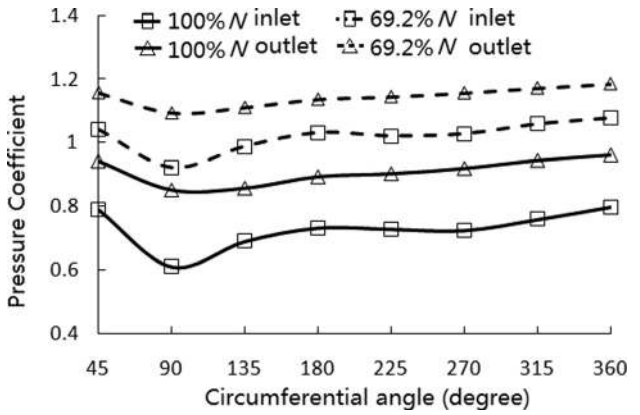

Fig. 6 Pressure coefficient distribution in the diffuser near surge

at approximately 90 deg downstream of the tongue at the diffuser outlet and inlet (as shown in Fig. 6), which is coincident with the results reported in Ref. [19]. It was considered to be caused by the perturbation at the volute tongue. The pressure coefficient distortion is quite different for the condition near choke, as shown in Fig. 7, where the pressure coefficient reaches the maximum value at around 90 deg, while it falls to the minimum value around 315 deg. The fluctuation in both situations is caused by the pressure perturbation across the tongue region.

A nondimensional parameter D_s was used to evaluate the magnitude of the distortion under different conditions

$$D_s = \frac{PC_{\max} - \overline{PC}}{\overline{PC}} \tag{2}$$

where $PC_{\max}$ is the maximum value of the pressure coefficient and $\overline{PC}$ is the circumferential area-averaged pressure coefficient for each operating point.

Figure 8 shows the magnitude of the pressure coefficient distortion in the diffuser near surge. It can be seen that the magnitude of the distortion at the diffuser inlet and outlet changes slightly with the rotational speeds near surge. For all rotational speeds, the magnitude of the distortion at the diffuser inlet is much larger than at the diffuser outlet. For the design rotational speed, D_s is 0.171 at the diffuser inlet, which is almost 2.4 times the magnitude of the distortion at the diffuser outlet. The experimental results showed that the absolute magnitude of the pressure coefficient distortion for the two locations is similar. However, the static pressure at the outlet is larger than at the inlet due to the diffusion. As a result, the parameter D_s is smaller for the outlet, as shown in the figure.

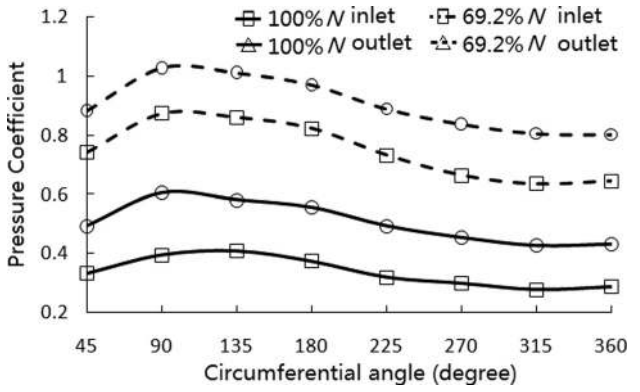

Fig. 7 Pressure coefficient distribution in the diffuser near choke

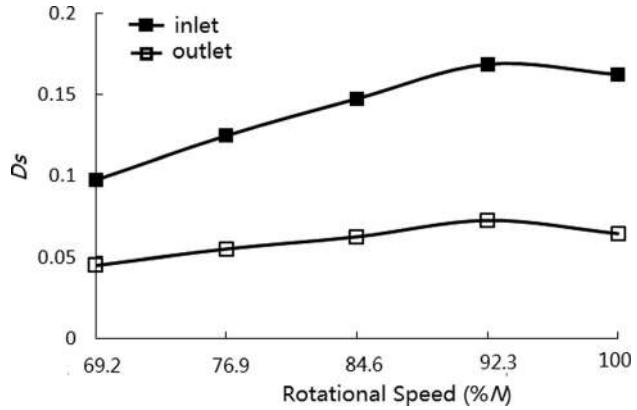

Fig. 8 Magnitude of the pressure coefficient distortion in the diffuser near surge

4.1.4 The Pressure Distribution in the Impeller. The static pressure distribution was further measured at the shroud near the leading edge of the main and splitter blades. Figure 9 shows the pressure coefficient near surge at the leading edge of the splitter blades for four rotational speeds.

The coefficient significantly varies in the circumferential direction at all rotational speeds viewed, yet with quite different patterns of disturbance. For the lower rotational speeds, i.e., 69.2% *N* and 84.6% *N*, there are two peaks in the circumference. The pressure coefficient has a minimum around 90 deg and 270 deg. For higher speeds, the magnitude of the distortion increases. At 100% *N* and 105% *N*, the distortion has a main wave length of 360 deg and remarkable amplitude. The pressure coefficient reaches a minimum value at about 220 deg for the former and 207 deg for latter. The magnitude of the fluctuation sharply increased as the rotational speed increases. It shall be noted that the patterns of the distortion are significantly different from those measured in the diffuser for the same speed and operation condition, as shown in Fig. 6, where there are no great differences in the pattern between low and high rotational speeds, although it is considered that the distortion in the impeller is due to the distortion at the inlet of the diffuser.

Figure 10 shows the pressure coefficient distribution near surge at the leading edge of the main blades near surge. The fact that the fluctuation of the pressure is much slighter than that near the leading edge of the splitter blades implies that the distortion is significantly suppressed by the upstream flow. However, the distortion still exists at the inlet of the main blades. This indicates that the distortion due to the asymmetrical geometry of the overhung volute can be propagated upstream from the diffuser outlet to the impeller inlet. The incidence, along with other flow parameters at the impeller inlet, is correspondingly variant in the circumferential direction, which will be shown in the latter part of the paper. Therefore, the impeller is subjected to varying inlet flow conditions although the upstream flow is uniform. Besides, when comparing the results shown in Figs. 9 and 10, the static pressure coefficient at the leading edges of the splitter blades is higher than that at the leading edges of the main blades, which indicates that the flow is diffused in the inducer near surge.

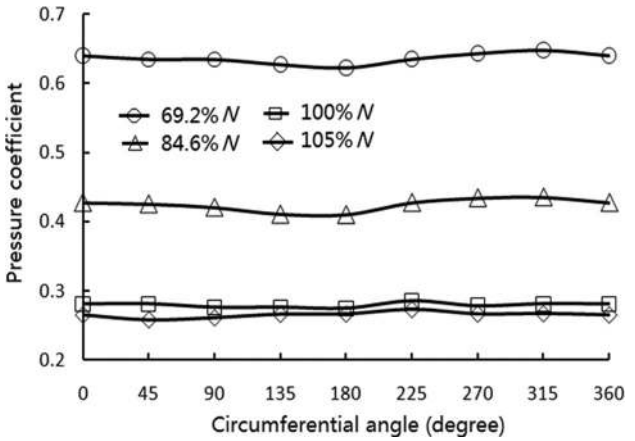

Fig. 10 Pressure coefficient distribution at the leading edge of the main blades near surge

Figures 11 and 12 show the pressure coefficient near choke at the leading edge of the splitter and main blades, respectively. The coefficient at the leading edge of the splitter blades for the four rotational speeds peaks between 180 deg and 225 deg. Similar to the near surge condition, the fluctuations of static pressure at the leading edge of the main blades are much less than that near the leading edge of the splitter blades. The distribution pattern at the splitter leading edge is notably different from the pattern near surge. Comparing the results shown in Figs. 11 and 12, the static pressure at the leading edge of the splitter blades is lower than that at the leading edge of the main blades, which indicates that the flow is accelerated in the inducer near choke.

4.1.5 The Distortion Phase Shift in the Impeller. Figure 13 shows the magnitude of the static pressure distortion at the leading edge of the splitter blades near surge. The magnitude of the distortion sharply increases as the rotational speed increases from 92.3% N *N* to 105% *N*. It should be noted that the magnitude in the diffuser does not tremendously increase. Different flow phenomenon exists in the impeller from the diffuser.

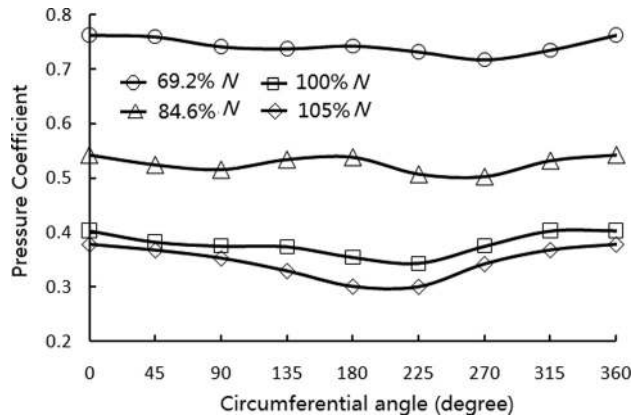

Fig. 9 Pressure coefficient distribution at the leading edge of the splitter blades near surge

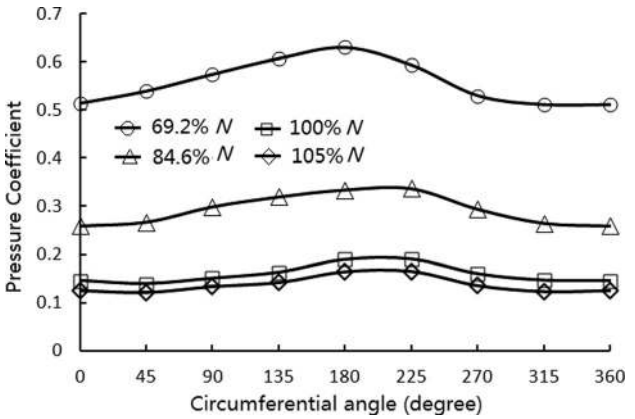

Fig. 11 Pressure coefficient distribution at the leading edge of the splitter blades near choke

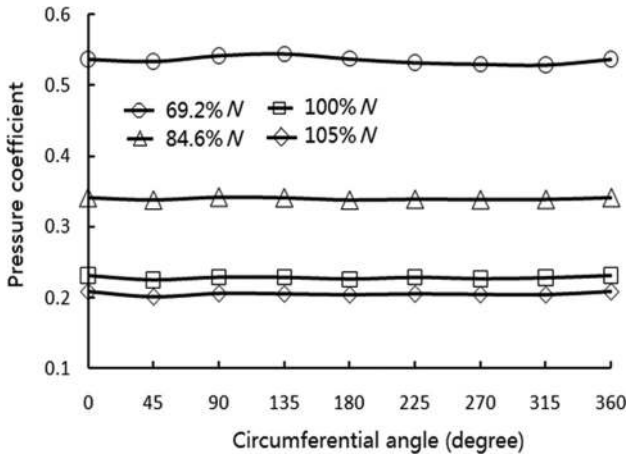

Fig. 12 Pressure coefficient distribution at the leading edge of the main blades near choke

According to the experimental measurement in the diffuser inlet, a distorted pressure is imposed at the impeller outlet. For a single passage in the impeller, a pulsed pressure is imposed at its outlet when the passage sweeps the distorted boundary. The frequency of the pulse is the rotational frequency. During a rotational cycle, the pulse will propagate inside the passage as a pressure wave. The unsteady interaction of the impeller and the volute could be characterized by the acoustic Strouhal number [11]. The number can be defined as follows

$$St = \frac{fL}{C} \tag{3}$$

Here, St represents the temporal relation between the rotation of the impeller and the perturbation wave propagation in the impeller. For the compressor investigated in this paper, f is defined as the rotational frequency, L is defined as the average length of the impeller passage in the streamwise direction, and C is defined as the speed of sound evaluated with, for convenience, the inlet temperature. When the periodicity of the perturbation and the wave propagation in the passages are the same, resonance happens. In this case, St is about 0.2 at 49.2% and 0.3 at 100%. Therefore, St will approach the case of resonance, i.e., $St = 0.5$, with increasing rotor speed. This results in an increasing amplitude of the distortion inside the passages as the rotational speed increases, as shown in Fig. 13.

A high pressure ratio compressor is likely to have a large St due to its larger size or higher rotational speed. Therefore, compared with the flow in a low pressure ratio compressor, the flow distortion in a high-pressure-ratio compressor impeller is expected to be much more severe and of utmost importance for consideration of the compressor performance and the flow stability.

Figure 14 shows the dimensionless pressure coefficient distribution at the diffuser inlet and the leading edge of the splitter blades near surge at a design rotational speed 105% N. In order to highlight the static pressure distribution, the pressure coefficient at different positions is dimensionless by its circumferential averaged values in order to eliminate the difference between the absolute values

$$\text{Dimensionless pressure coefficient} = \frac{PC}{\overline{PC}} \tag{4}$$

It can be seen that there is a phase shift of about 110 deg in the distortion from the impeller outlet (diffuser inlet) to the leading edge of the splitter blades. A numerical simulation of a low-pressure-ratio compressor was performed to investigate the interaction between the impeller and volute before [19], and it was found that flow distortion at the outlet and inside of the impeller is present in the passages downstream of the tongue. The blade wrap angle was responsible for a part of the phase shift between the trailing and leading edge, however, it is obviously not large enough to be the single cause of the phenomenon. As discussed before, the St of the compressor is larger than 0.1, which means that the unsteady effects are not ignorable. The pressure perturbation propagates at the local speed of sound in the relative frame. Therefore, when it propagates upstream in the passage, i.e., from outlet to inlet, the relative velocity is $C - W$ upstream in the rotating frame and $C + W$ when it is reflected and travels downstream (W is the relative flow velocity). The average velocity of propagation can be simplified by the speed of sound C. Therefore, the time it takes for the distortion wave to travel from the trailing edge to the splitter leading edge is evaluated as follows

$$t = \frac{L}{C} \tag{5}$$

For the investigated compressor, t is about 0.18 ms. During this short time, the rotation angle of the impeller is about 70 deg at the design rotational speed. The discrepancies between the evaluation and the experimental results can be induced by the evaluation of the propagation velocity and the passage length. It could be seen that the influence of the rotation of the impeller on the phase shift of the distortion is much larger than the effect of the wrap angle. Therefore, the propagation of the disturbance wave and the meanwhile rotation of the impeller are the two main reasons for the phase shift of the distortion from the outlet upstream into the impeller.

4.2 Flow Simulation. As previously discussed, the Strouhal number of the compressor at design speed is about 0.3. Therefore,

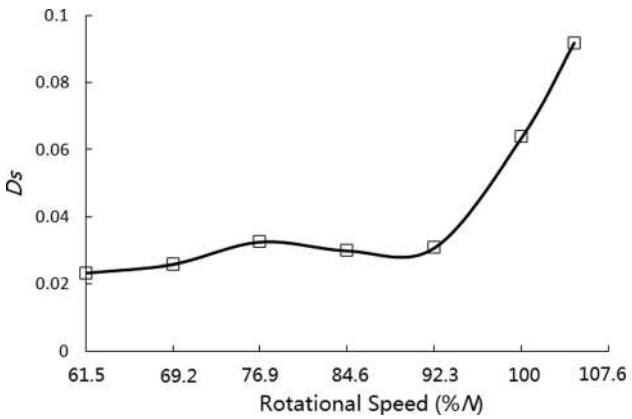

Fig. 13 Magnitude of the pressure coefficient distortion at the leading edge of the splitter blades near surge

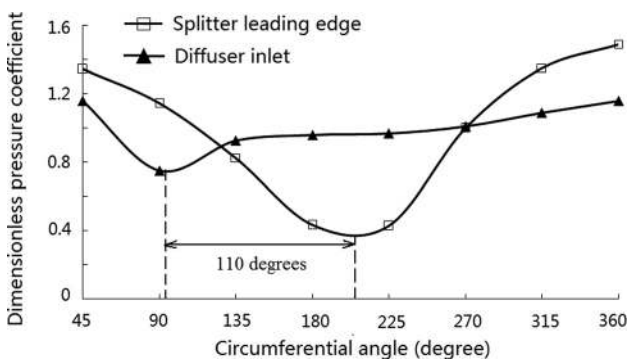

Fig. 14 Static pressure distribution at the diffuser inlet and the leading edge of the splitter blades near surge at 105% *N*

the unsteady effect of propagation of the disturbance wave is significant in the impeller because of its rotation. However, the steady state numerical method can still be used to investigate the circumferential asymmetric flow field in the compressor which is caused by the volute, although the phase shift between the outlet and passages of the impeller will inevitably not be correctly predicted. The steady state simulation can be considered as a case in which the velocity of the disturbance propagation is so large that the time needed for propagation can be ignored.

The numerical simulation has to be validated by experimental results; therefore, the compressor performance is compared in Fig. 15. The mass flow is normalized by the designed flow rate. Figure 15 shows that the averaged total to total pressure ratio (Fig. 15(*a*)) by the simulation is around 6.7% higher than by the experiment at the designed speed while the predicted efficiency (Fig. 15(*b*)) is 3.2% lower than the experimental results. Several factors may induce the discrepancies between the simulation and experiment, including the turbulence model, a nonaccurate tip model, the surface roughness (i.e., volute inner surface), etc. [20]. Some differences exist in the surge point and choke point by the simulation and the experimental measurement. The discrepancies between the model and real geometries may induce the errors. The flow could be choked near the leading edge of the splitter where the throat is located. The error of the modeled geometries near the splitter leading edge may induce the error of the predicted choke flow rate. Especially, the predicted surge point is taken by the failure of the simulation convergence. In the models established in the paper, the inlet and outlet ducts are not modeled for simplification which, together with the factors mentioned before, may induce the difference on the surge point. In spite of the discrepancies, the predicted results are moderately in accordance with the experimental results. Further flow field investigations should be reasonably based on the numerical method.

Figure 16 shows the comparison of the dimensionless pressure coefficient distribution in the circumferential direction at the outlet and inlet of the diffuser between the simulation and the experiment (defined by Eq. (4)), both near surge condition at 100% *N*. According to the results shown in Fig. 15, it is inferred that some differences exist between the flow parameters by prediction and experiment. A static pressure distortion can be seen at the approximately 90 deg circumferential angle for both the simulation and the experiment. Although the discrepancies exist between two results, the predicted and measured phase of distortion are in accordance with each other, which further indicates that the numerical simulation used is reasonable to predict the asymmetric characteristics of the flow field in the diffuser.

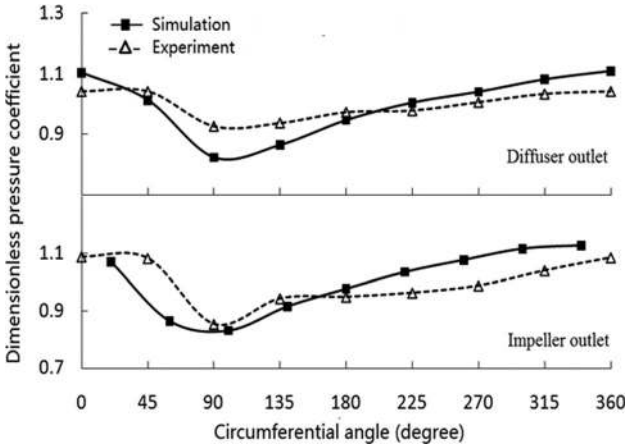

Fig. 16 Pressure coefficient distributions comparison in the diffuser near surge at 100% *N*

Figure 17 compares the circumferential distribution of the pressure coefficient by simulation and experiment at the leading edge of the splitter blades near surge at the design rotational speed. In the simulation results, a pressure distortion exists at around 100 deg, which is approximately coincident with the distortion phase at the impeller outlet. A similar phenomenon was reported in Refs. [11,12]. However, it can be seen that there is a large phase shift (about 120 deg) between the simulation and experiment results. It implied that the steady state simulation cannot be used to predict the phase shift of the distortion; *St* is zero in the steady state simulation. However, the actual *St* is up to 0.3 at the design rotational speed and unsteady effects cannot be neglected.

Although steady state simulation cannot be used to predict the phase shift in the impeller, the shapes of the static pressure distribution by simulation and experiment are similar. The numerical steady simulation neglects the aforementioned unsteady effects found in the experiments, but facilitates a detailed analysis of the asymmetric flow field in the impeller.

Figure 18 shows the flow rate, the inlet relative flow angle, and the outlet static pressure distribution of each passage near surge at

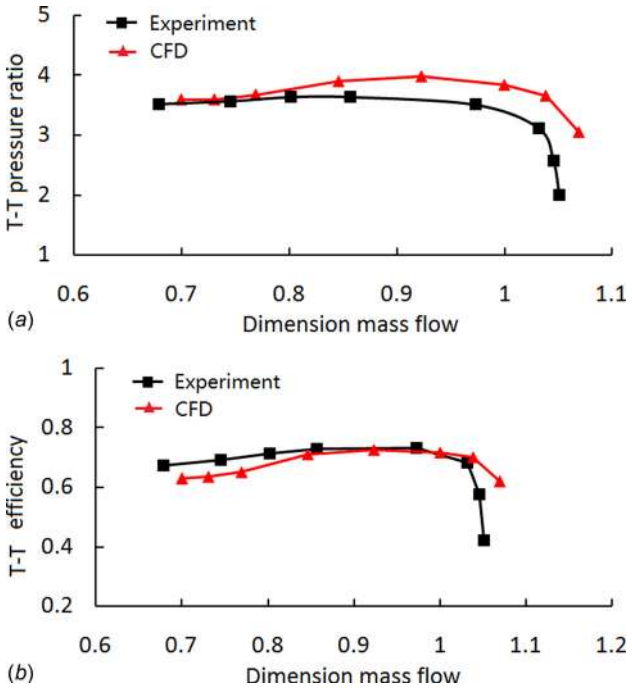

Fig. 15 Comparison of the performance of the experiment and numerical simulation at 100% *N*: (*a*) total to total pressure ratio, and (*b*) total to total efficiency

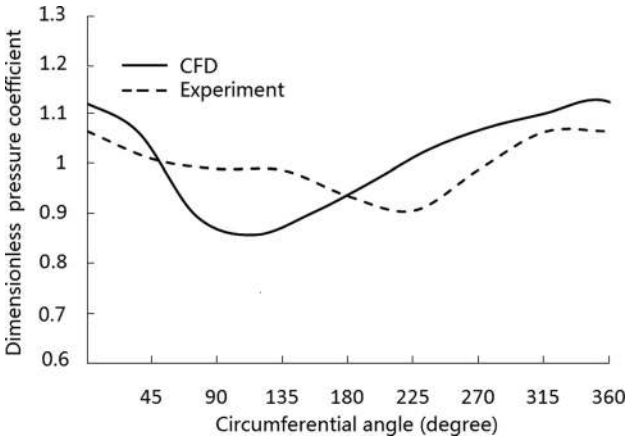

Fig. 17 Pressure coefficient distribution in the circumferential direction near the leading edge of the splitter blades near surge at 100% *N*

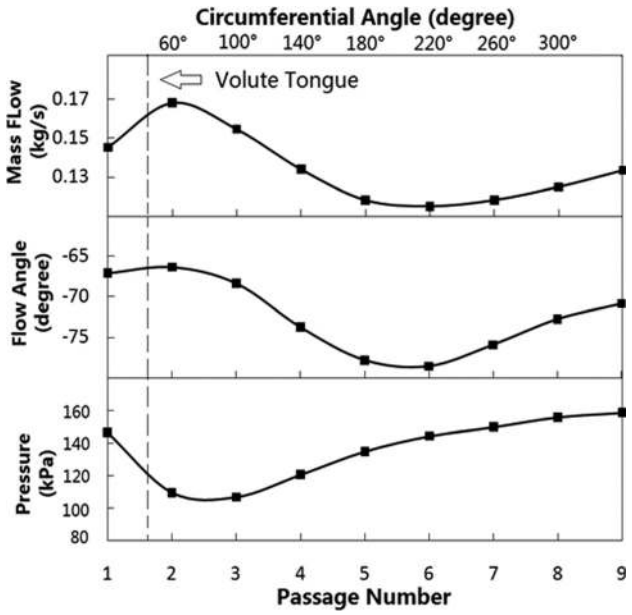

Fig. 18 Flow parameters distribution in the impeller passages near surge at 100% *N*

the design rotational speed. The abscissa is the circumferential degrees and passage number, which can be seen in Fig. 1(*c*). All three flow parameters vary from passage to passage. The flow rate peaks in the second passage and falls to the minimal value in passage 6. Since the axial velocity component at the impeller inlet varies in the same way as the flow rate, the distribution of the inlet flow angle is similar to that of the flow rate. The variation of the flow rate in the passages can be explained, to some extent, by the pressure distribution at the outlet of the impeller since the passage with a larger adverse pressure gradient exhibits a smaller flow rate. However, the relation between the minimum mass flow and maximum static pressure is not so straightforward between the flow rate characteristic and the outlet static pressure distribution. The flow rate and inlet flow angle falls to the lowest value at passage 6, where the outlet static pressure does not reach its maximum value.

Figure 19 shows the static pressure distribution near the tip of the impeller blades near surge at design rotational speed. It can be seen that the pressure distribution in the impeller passage is quite different because of the difference in the structure of the supersonic/transonic zone at the leading edge of the main blades. It is the flow rate and incidence that changes the velocity distribution and therewith, the flow acceleration in each passage.

Figure 20 shows the relative Mach number near the tip of the impeller blades near surge at the design rotational speed. The largest part of the suction surface is covered by low momentum flow in passage 6, in which the flow rate is the least among the passages (Fig. 20(*b*)). On the contrary, the flow in passages 2, 1, and 9 are similar to that at a normal condition near the design condition, as shown in Fig. 20(*a*). The basic reason for impeller stall is the large incidence, which will cause blade surface flow separation, strong leakage flow, and other kinds of deteriorated flow in the passage. According to the predicted flow angle distribution in the passages (Fig. 18), it can be inferred that stall first happens in passage 6 in the steady picture. The propagation of the distortion in the passage and the revolution of the impeller might make the steady picture shift around 110 deg in the rotating direction in an unsteady picture, which has been analyzed before. In spite of

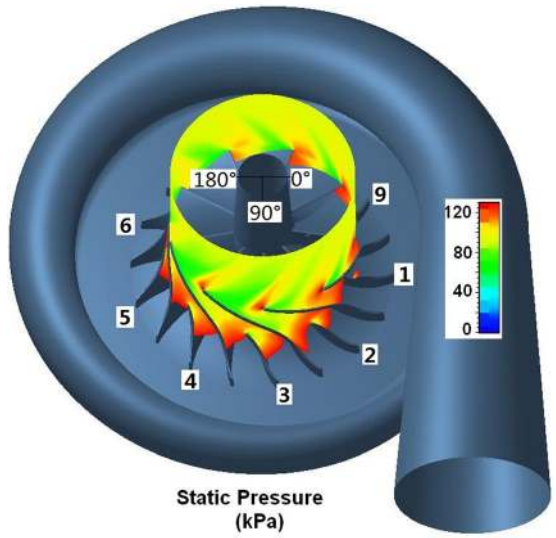

Fig. 19 Static pressure distribution near the tip of the impeller blades near surge at 100% *N*

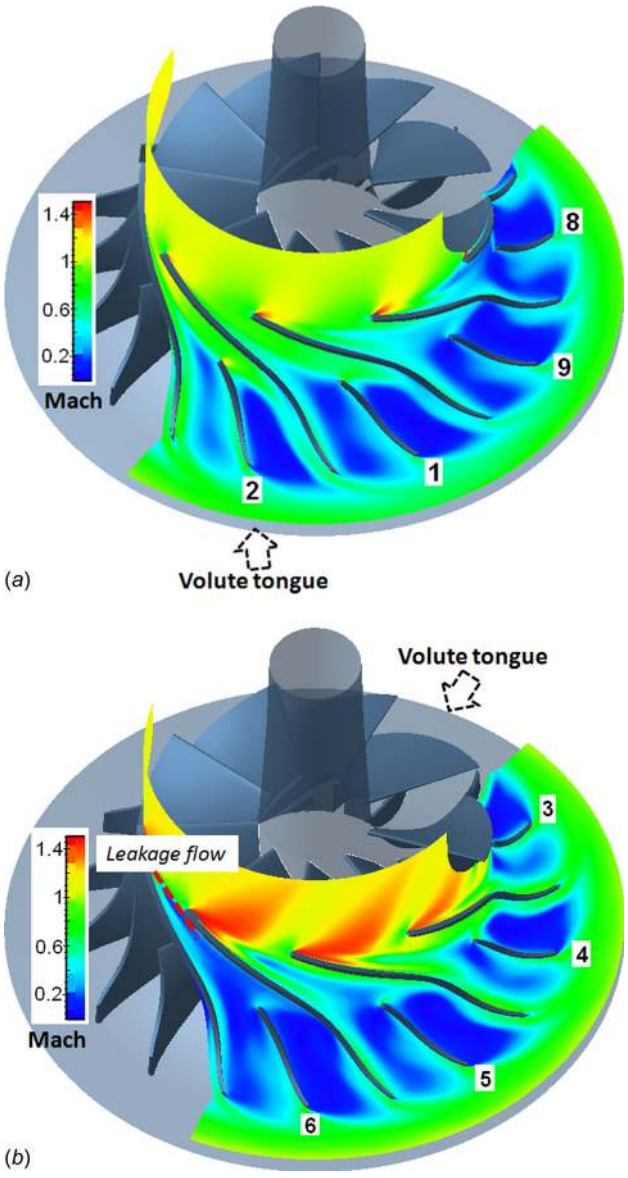

Fig. 20 Relative Mach number distribution near the tip of the impeller blades near surge at 100% *N*:(*a*) passages 8, 9, 1, and 2, and(*b*) passages 3, 4, 5, and 6

this shifting, the results from the steady simulation should be reasonable in a qualitative analysis. The unsteady picture could be enlightened by shifting the steady results in the circumferential direction. It can be further implied that the passages with flow distortion will be more likely to stall at a higher pressure ratio than at a lower pressure ratio because of the larger amplitude of distortion. Obviously, a treatment for stability improvement concentrating in this zone will be more efficient.

5 Conclusions and Remarks

The nonaxisymmetrical flow in a high-pressure-ratio turbocharger centrifugal compressor was studied. The static pressure distribution in the streamwise direction in the compressor was measured and analyzed. Conclusions could be drawn from the experiments as follows:

1. There is an evident nonaxisymmetrical flow pattern throughout the compressor due to the asymmetric geometry of the overhung volute. The static pressure field in the diffuser is distorted at approximately 90 deg in the rotational direction downstream of the volute tongue throughout the diffuser. The magnitude of this distortion slightly varies with the rotational speeds.
2. The magnitude and shape of the static pressure distortion in the impeller is a function of the rotational speed. The magnitude of the distortion sharply increases as the rotational speed goes up to 105% N. There are two valley values in the static pressure circumferential distribution at lower speeds, while there is only one at higher speeds.

   The numerical steady state simulation neglects the aforementioned unsteady effects found in the experiments, however, it facilitates a detailed analysis of the asymmetric flow field in the impeller, allowing the identification of the passages responsible for the inception of inducer stall. It can be concluded as follows:
3. The flow rate among impeller passages is nonuniformly distributed due to the distorted static pressure distribution at the outlet of the impeller. Thus, the circumferential distribution of the inlet flow angle is distorted and the flow pattern in each passage is different.

Since the flow pattern among passages varies from one to the other, the discrepancy of the stability of the passages could be induced. A flow control method targeted at stability improvement is more proper to be designed differently for different passages. Based on the detailed study of the nonaxisymmetrical flow field induced by the volute, Part II of this two-part paper will develop an asymmetric flow control method to widen the stable flow range of the high-pressure-ratio turbocharger centrifugal compressor.

Acknowledgment

This research was supported by the National Natural Science Foundation of China (Grant No. 51176087).

Nomenclature

A/R = ratio of volute throat area to its radius
C = speed of sound
C_p = specific heat at constant pressure
D_s = magnitude of static pressure distortion
f = impeller rotational frequency
L = characteristic length in the Strouhal number
N = design rotational speed
P = static pressure
PC = pressure coefficient
St = Strouhal number
t = time
T^* = total temperature
T-T = total to total (pressure ratio or efficiency)
U = impeller rotational velocity
W = relative flow velocity
ρ = gas density

Subscripts

1 = impeller inlet
2 = impeller outlet
5 = diffuser outlet
in = inlet
max = maximum

References

[1] Baines, N. C., 2005, "Fundamentals of Turbochargers," Concepts ETI, Inc., Vermont.
[2] Hawley, J. G., Wallace, F. J., Cox, A., Horrocks, R. W., and Bird, G. L., 1999, "Variable Geometry Turbocharging for Lower Emissions and Improved Torque Characteristics," Proc. Inst. Mech. Eng., Part D, J. Automob. Eng., **213**(2), pp. 145–159.
[3] Clenci, A. C., Descombes, G., Podevin, P., and Hara, V., 2007, "Some Aspects Concerning the Combination of Downsizing with Turbocharging, Variable Compression Ratio, and Variable Intake Valve Lift," Proc. Inst. Mech. Eng., Part D, J. Automob. Eng., **221**(10), pp. 1287–1294.
[4] Maiboom, A., Tauzia, X., and Héteta, J. F., 2008, "Experimental Study of Various Effects of Exhaust Gas Recirculation (EGR) on Combustion and Emissions of an Automotive Direct Injection Diesel Engine," Energy, **33**(1), pp. 22–34.
[5] Rodgers, C., 2001, "Turbocharging a High Altitude UAV C.I. Engine," AIAA Paper No. 2001-3970.
[6] Krain, H., Karpinski, G., and Beversdorff, M., 2001, "Flow Analysis in a Transonic Centrifugal Compressor Rotor Using 3-Component Laser Velocimetry," ASME Paper No. 2001-GT-0315.
[7] Ayder, E., and Van den Braembussche, R. A., 1991, "Experimental Study of the Swirling Flow in the Internal Volute of a Centrifugal Compressor," ASME Paper No. 91-GT-7.
[8] Ayder, E., and Van den Braembussche, R. A., 1994, "Numerical Analysis of the Three-Dimensional Swirling Flow in Centrifugal Compressor Volutes," ASME J. Turbomach., **116**(2), pp. 462–468.
[9] Ayder, E., Van den Braembussche, R. A., and Brasz, J. J., 1993, "Experimental and Theoretical Analysis of the Flow in a Centrifugal Compressor Volute," ASME J. Turbomach., **115**(3), pp. 582–589.
[10] Gu, F. H., Engeda, A., Cave, M., and Liberti, J. L. D., 2001, "A Numerical Investigation on the Volute/Diffuser Interaction Due to the Axial Distortion at the Impeller Exit," ASME Journal of Fluids Engineering, **123**(3), pp. 475–483.
[11] Gu, F. H., and Engeda, A., 2001, "A Numerical Investigation on the Volute/Impeller Steady-State Interaction due to Circumferential Distortion," ASME Paper No. 2001-GT-0328.
[12] Hillewaert, K. and Van den Braembussche, R. A., 1999, "Numerical Simulation of Impeller-Volute Interaction in Centrifugal Compressors," ASME J. Turbomach., **121**(3), pp. 603–608.
[13] Reunanen, A., Pitkanen, H., Siikonen, T., Heiska, H., Larjola, J., Esa, H., and Sallinen, P., 2000, "Computational and Experimental Comparison of Different Volute Geometries in a Radial Compressor," ASME Paper No. 2000-GT-469.
[14] Sorokes, J., Borer, C., and Koch, J., 1998, "Investigation of the Circumferential Static Pressure Non-Uniformity Caused by a Centrifugal Compressor Discharge Volute," ASME Paper No. 98-GT-326.
[15] Hagelstein, D., Van den Braembussche, R., Keiper, R., and Rautenberg, M., 1997, "Experimental Investigation of the Circumferential Pressure Distortion in Centrifugal Compressor Stages," ASME Paper No. 97-GT-50.
[16] Fatsis, A., Pierret, S., and Van den Braembussche R. A., 1997, "Three Dimensional Unsteady Flow and Forces in Centrifugal Impellers with Circumferential Distortion of the Outlet Static Pressure," ASME J. Turbomach., **119**(1), pp. 94–102.
[17] Spalart, P. R., and Allmaras, S. R., 1992, "A One Equation Turbulence Model for Aerodynamic Flows," AIAA Paper No. 92-0439.
[18] Guo, G. D., Zhang, Y. J., Xu, J. Z., Zheng, X. Q., and Zhuge, W. L., 2008, "Numerical Simulation of a Transonic Centrifugal Compressor Blades Tip Clearance Flow of Vehicle Turbocharger," ASME Paper No. GT2008-50957.
[19] Hagelstein, D., Hillewaert, K., and Van den Braembussche, R. A., 2000, "Experimental and Numerical Investigation of the Flow in a Centrifugal Compressor Volute," ASME J. Turbomach., **122**(1), pp. 22–31.
[20] Denton J. D., 2010. "Some Limitations of Turbomachinery CFD," ASME Paper No. GT2010-22540.